Published in Environmental Modelling & Software 26, issue 7, 886-898, 2011
which should be used for any reference to this work

A hydraulic mixing-cell method to quantify the groundwater component of streamflow within spatially distributed fully integrated surface water–groundwater flow models

D. Partington [a,*], P. Brunner [b], C.T. Simmons [c,1], R. Therrien [d], A.D. Werner [c], G.C. Dandy [a,2], H.R. Maier [a,3]

[a] School of Civil, Environmental and Mining Engineering, The University of Adelaide, Adelaide, South Australia 5005, Australia
[b] Centre of Hydrogeology and Geothermics (CHYN), Rue Emile-Argand 11, CP 158, CH-2009 Neuchâtel, Switzerland
[c] School of the Environment and National Centre for Groundwater Research and Training, Flinders University, GPO Box 2100, Adelaide, South Australia 5001, Australia
[d] Department of Geology and Geological Engineering, Université Laval, Quebec, Canada G1K 7P4

ABSTRACT

The complexity of available hydrological models continues to increase, with fully integrated surface water–groundwater flow and transport models now available. Nevertheless, an accurate quantification of streamflow generation mechanisms within these models is not yet possible. For example, such models do not report the groundwater component of streamflow at a particular point along the stream. Instead, the groundwater component of streamflow is approximated either from tracer transport simulations or by the sum of exchange fluxes between the surface and the subsurface along the river. In this study, a hydraulic mixing-cell (HMC) method is developed and tested that allows to accurately determine the groundwater component of streamflow by using only the flow solution from fully integrated surface water–groundwater flow models. By using the HMC method, the groundwater component of streamflow can be extracted accurately at any point along a stream provided the subsurface/surface exchanges along the stream are calculated by the model. A key advantage of the HMC method is that only hydraulic information is used, thus the simulation of tracer transport is not required. Two numerical experiments are presented, the first to test the HMC method and the second to demonstrate that it quantifies the groundwater component of streamflow accurately.

Keywords
Surface water–groundwater interaction, HydroGeoSphere, Streamflow generation

1. Introduction

A quantitative understanding of streamflow hydrographs is an important precondition to the understanding and effective management of any catchment (VanderKwaak and Loague, 2001; Jones et al., 2006; Mirus et al., 2009). The streamflow hydrograph is generated by different mechanisms such as groundwater discharge to the stream, discharge from the unsaturated zone, overland flow, preferential flow through macropores and/or fractures, and direct precipitation to the stream. These streamflow generation components can exhibit complex spatial and temporal behaviour. This complexity makes it difficult to easily decompose streamflow hydrographs in terms of streamflow generation mechanisms if one or several components of the hydrograph are unknown. Groundwater discharge is a critical streamflow generation component that is difficult to quantify. The quantitative assessment of the groundwater component of streamflow (which represents the quantity of streamflow at a given point in space and time derived from groundwater discharging directly to the stream) is of great importance in understanding catchment hydrology and informing water resources management, as highlighted by Sophocleous (2002) and Winter (1999). Accurate simulation of the groundwater component of streamflow is therefore important in hydrological modelling exercises (e.g. Gilfedder et al., 2009; Croton and Barry, 2001; Facchi et al., 2004) in order to inform water resources management.

The groundwater component of streamflow cannot be measured easily in the field (Hattermann et al., 2004; McCallum et al., 2010) and therefore is usually quantified using indirect methods. Indirect methods can involve the use of environmental

* Corresponding author. Tel.: +61 8 8303 4323; fax: +61 8 8303 4359.
E-mail addresses: dparting@civeng.adelaide.edu.au (D. Partington), philip.brunner@unine.ch (P. Brunner), craig.simmons@flinders.edu.au (C.T. Simmons), rene.therrien@ggl.ulaval.ca (R. Therrien), adrian.werner@flinders.edu.au (A.D. Werner), gdandy@civeng.adelaide.edu.au (G.C. Dandy), hmaier@civeng.adelaide.edu.au (H.R. Maier).
[1] Tel.: +61 8 8201 5509; fax: +61 8 8201 7906.
[2] Tel.: +61 8 8303 4139; fax: +61 8 8303 4359.
[3] Tel: +61 8 8303 5472; fax: +61 8 8303 4359.

and conservative tracers for separation of the hydrograph (McGlynn and McDonnell, 2003; McGuire and McDonnell, 2006), and recession analysis based on conceptual storage–discharge relationships for the catchment (Chapman, 2003; Eckhardt, 2008). However, as pointed out by Hewlett and Troendle (1975), 'the accurate prediction of the hydrograph implies adequate modelling of the sources, flowpaths and residence time of water'. In particular, capturing the flowpaths requires a spatially distributed model. Unless the assumptions of the indirect methods can be resolved or justified, the adequate modelling of sources and flowpaths of water is insufficient. If the modelling is insufficient, then it follows that the separation of the hydrograph may be meaningless. Given the difficulty faced in accurately measuring sources and flowpaths within hillslopes, let alone entire catchments, some benefit can be found in examining hypotheses which can be adequately 'measured' in the 'virtual laboratory' (Weiler and McDonnell, 2004).

One could expect that the tools for quantifying the groundwater component of streamflow are now readily available in the latest generation of fully integrated spatially distributed models such as InHM (VanderKwaak and Loague, 2001), MODHMS (HydroGeoLogic, 2006), HydroGeoSphere (HGS) (Therrien et al., 2009), Wash123D (Cheng et al., 2005) and ParFlow (Kollet and Maxwell, 2006). However, this is not the case. Even within spatially distributed numerical models, quantifying source components remains a challenge (Sayama and McDonnell, 2009). The same applies to the ultimate delivery mechanisms as defined in Sklash and Farvolden (1979). Because the currently available numerical models do not report the groundwater component of streamflow at a given location, it is often approximated by introducing tracers or by setting it equal to the summed exfiltration along a section or entire length of the stream. The summed exfiltration is defined in this paper as the sum of all fluxes from the subsurface to the stream at a specific point in time upstream of the point at which the hydrograph is measured.

The aforementioned approaches are problematic. For example, the summed exfiltration during a simulation is not equal to the groundwater component of streamflow at the same simulation time. This can be attributed to the fact that portions of the summed exfiltration exhibit a time lag from the point of entering the stream to the point of streamflow measurement, as a result of potentially significant transit times within stream networks (McGuire and McDonnell, 2006). This time lag cannot be captured if the groundwater component of streamflow is approximated by the summed exfiltration. Furthermore, if the stream loses water to the subsurface between a point of groundwater discharging into the stream and the point where the hydrograph is measured, only a portion of the groundwater entering the stream will contribute to the groundwater component of streamflow at the point of hydrograph measurement. In that case, the summed exfiltration will overestimate the groundwater component of streamflow at the point of hydrograph measurement.

In this study, a mixing-cell method for quantifying the groundwater component of streamflow in fully integrated spatially distributed models is described. Mixing-cell models have often been used in hydrogeology to model solute transport (Adar et al., 1988; Campana and Simpson, 1984). Mixing-cell models rely only on conservation of mass. The hydraulic mixing-cell (HMC) method described in this study relies on hydraulic information only (i.e. fluxes). Moreover, the method allows tracking streamflow generation mechanisms at every cell or element within the stream of the model domain. Therefore, complex spatial and temporal effects are captured and can be accounted for. The method is developed and tested using a particular numerical model (HydroGeoShpere, Therrien et al., 2009), but it can be implemented to any code that reports the exchange between the subsurface and surface in a spatially distributed manner. The paper also aims to explore the suitability of traditional methods (e.g. equilibrating the groundwater component of streamflow to the summed exfiltration) for quantifying the groundwater component of streamflow within numerical models.

2. Existing methods for extracting streamflow generation components

The hypothetical catchment shown in Fig. 1 is used to illustrate the challenges of extracting the groundwater component of streamflow from numerical models using existing methods. In the catchment shown, the stream, which is flowing from A to B to C, is gaining in sections A and C, but losing in section B.

2.1. Summed exfiltration along the length of the stream

For each of cross sections A, B and C of the hypothetical catchment shown in Fig. 1, the expected streamflow hydrograph is

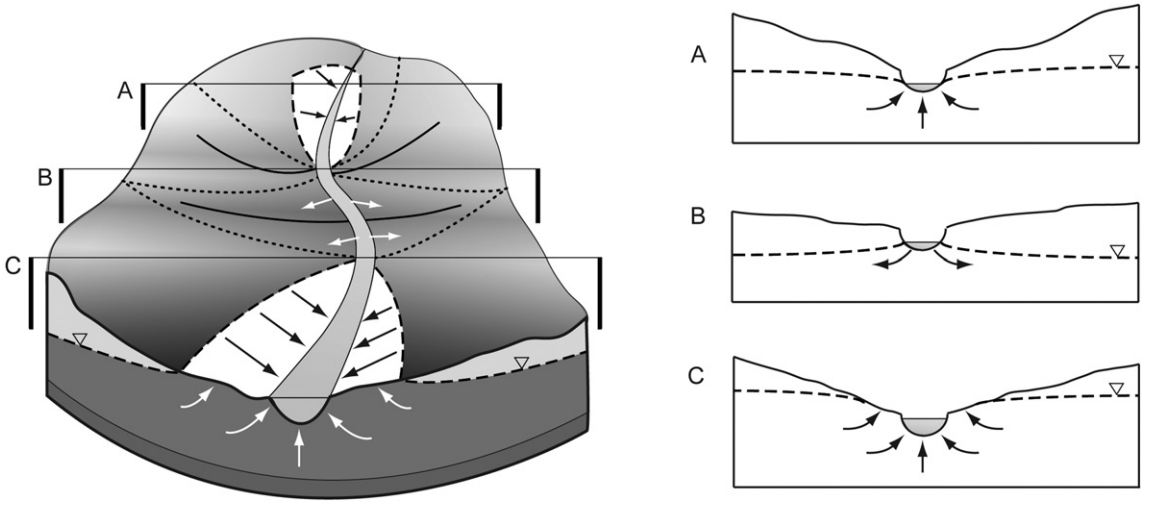

Fig. 1. Conceptual diagram of a surface water–groundwater catchment (left hand side) featuring different flow regimes (as illustrated in the right part of the figure). The white sections of the catchment adjacent to the stream represent the groundwater discharge upslope of the stream (return flow). The dashed lines on the right part of the figure represent the water table. The flow direction is towards the reader.

shown in Fig. 2, along with the groundwater component of streamflow and the summed exfiltration. The streamflow in Fig. 2A, B and C refers to the point measurement at each of cross sections A, B and C. Although the results shown in Fig. 2 are hypothetical, they illustrate the following two problems that arise by approximating the groundwater component of the streamflow using the summed exfiltration:

1) The summed exfiltration does not account for the time lag between the upstream points of groundwater discharging from the aquifer to the stream and the point where the hydrograph is measured, as illustrated by the time lag between the summed exfiltration and the groundwater component of streamflow curves. The streamflow travel times for the summed exfiltration upstream of cross sections A, B and C actually correspond to the time lag between the peaks of the summed exfiltration and the streamflow hydrograph in Fig. 2.
2) Changing flow regimes cannot be considered correctly. When a part of the stream is losing and other parts are gaining, the summed exfiltration is not equal to the groundwater component of streamflow at a particular location, even if the aforementioned time lag is negligible.

The effect of ignoring time lags and discounting losses along the stream becomes clear when moving downstream from cross sections A to B to C. For example, the course of the groundwater component of streamflow at cross section A features a flatter and broader distribution through time compared to the summed exfiltration upstream of A. When considering the streamflow hydrograph at cross section C in Fig. 2, the significance of time lags, particularly from the most upstream sub-catchments, becomes apparent.

2.2. Tracer based hydrograph separation

The use of conservative tracers within models provides temporal information on the original source of water (i.e. groundwater, soil water, rainfall). Whilst the application of solutes is extremely useful in identifying the source of streamflow, it gives no real indication of the mechanism of streamflow generation (McGuire and McDonnell, 2006). Even with temporal information on the source of water, the parameters associated with tracer transport (i.e. diffusion, tortuosity and dispersivity) often affect the interpretation of the source as demonstrated in Jones et al. (2006). Jones et al. (2006) found that the value of dispersivity used in simulating the transport of tracers could lead to large overestimation of the pre-event water's contribution to streamflow. In their model using InHM of the Borden rainfall–runoff experiment, the pre-event contributions to streamflow using longitudinal dispersion $\alpha_L = 0.5$ m and 0.005 m were found to be 41.6% and 33.9%, respectively, with the hydraulically based subsurface contribution close to 0%. These results would suggest that in the streamflow hydrograph in Fig. 1 at cross section C of the catchment, the groundwater component of streamflow could be easily overestimated using tracers as illustrated in Fig. 3.

Given such large variation in the tracer based interpretations of groundwater contributions to streamflow, it seems quite clear that inherent accuracy relies on reliability and certainty of the transport parameters. Any uncertainty in the dispersivity directly relates to uncertainty in quantifying the groundwater component of streamflow. Therefore quantifying the groundwater component of the streamflow hydrograph within models using tracers may be undermined by large uncertainty.

3. A hydraulic balance using a hydraulic mixing-cell method

The hydraulic mixing-cell (HMC) method introduced in this paper allows the streamflow generation mechanisms to be deconvoluted from the streamflow hydrograph at any point along the stream. The method relies on standard hydraulic output from numerical models only. It is based on the modified mixing cell of Campana and Simpson (1984). Furthermore, it is assumed for the simplicity of coding that the width of the stream does not change during the simulation and additionally that the flow direction in the stream does not change. This mass balance of the HMC method is verified by application to two numerical test cases using HydroGeoSphere. The method can be generalised to any spatially distributed surface water–groundwater code, as mentioned previously.

3.1. Theory

The numerical modelling of streamflow requires discretisation over space and time of the relevant governing flow equation using a finite difference (FD), finite volume (FV) or finite element (FE) scheme. The method developed herein is designed to fit in accordingly with existing numerical models.

Consider the continuity of flow for a stream cell i of arbitrary shape. This can be expressed in terms of the streamflow generation/depletion as:

$$Q_{Up} \pm Q_{GW} \pm Q_{OF} \pm Q_{UF} \pm Q_{PF} + Q_{Rain} - Q_{Down} - Q_{Evap} = \frac{dV}{dt} \quad (1)$$

where Q_{Up} [L^3/T] is the upstream flow (generated from groundwater, overland flow, unsaturated flow and rainfall) into the stream cell; Q_{GW}, Q_{OF}, Q_{UF} and Q_{PF} [L^3/T] are the groundwater, overland flow, unsaturated flow and preferential flow, respectively, flowing into or out of the cell; Q_{Rain} [L^3/T] is the rainfall contribution to the stream cell, Q_{Down} is the flow downstream (generated from groundwater, overland flow, unsaturated flow and rainfall) flowing out of the cell [L^3/T]; Q_{Evap} [L^3/T] is the loss of water from storage (composed of groundwater, overland flow, unsaturated flow and rainfall) due to

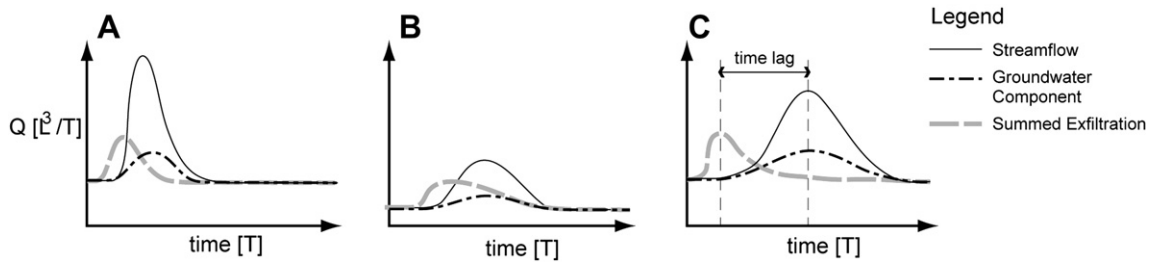

Fig. 2. Hydrograph at cross sections A, B and C of the catchment shown in Fig. 1. The streamflow and corresponding component of groundwater flowing through cross sections A, B and C are shown. Also, the summed exfiltration upstream of cross sections A, B and C, respectively, is shown.

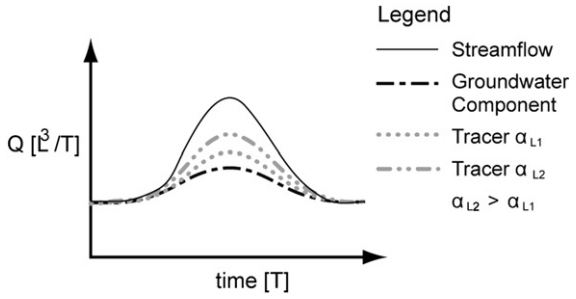

Fig. 3. The theoretical hydrograph at cross section C of the catchment shown in Fig. 1. The streamflow, groundwater discharge component and tracer based separation (for dispersivity values of α_{L1} and α_{L2}) are shown.

evaporation; dV/dt [L^3/T] is the rate of change of storage within the cell.

More concisely the fluid mass balance for a particular cell i with neighbouring cells j in the surface domain can be written as:

$$\sum_{j=1}^{n} Q_{ji} - \sum_{j=1}^{m} Q_{ij} = \frac{dV_i}{dt} \tag{2}$$

where Q_{ji} [L^3/T] is the jth flux into the cell i; Q_{ij} [L^3/T] is the jth flux out of the cell i; V_i [L^3] is the volume in cell i; t [T] is time; and n and m denote n sources and m sinks.

By multiplying (2) by dt and integrating both sides over the interval t_1 to t_2, $(t_2 > t_1)$ we obtain the following:

$$V_{t_2} - V_{t_1} = \int_{t_1}^{t_2} \sum_{j=1}^{n} Q_{ji} dt - \int_{t_1}^{t_2} \sum_{j=1}^{m} Q_{ij} dt \tag{3}$$

$$V_{t_2} = V_{t_1} + \sum_{j=1}^{n} V_{ji}\Big|_{t_1}^{t_2} - \sum_{j=1}^{m} V_{ij}\Big|_{t_1}^{t_2} \tag{4}$$

For each cell the discrete volumetric balance over each time step dt can be written:

$$V_i^N = \sum_{k=1}^{K} V_{i(k)}^N \quad \text{for } K \text{ streamflow components} \tag{5}$$

where V_i^N [L^3] is the total volume of water in cell i at time N; $V_{i(k)}^N$ [L^3] are the volumes of groundwater flow, unsaturated flow, overland flow, preferential flow and direct rainfall water, respectively, in cell i at time N. These constituent balances are defined as:

$$V_{i(k)}^N = V_{i(k)}^{N-1} + \sum_{j=1}^{n} V_{ji(k)}\Big|_{N-1}^{N} - \sum_{j=1}^{m} V_{ij(k)}\Big|_{N-1}^{N} \tag{6}$$

where $V_{ji(k)}$ and $V_{ij(k)}$ [L^3] are the volumes of the k^{th} component of streamflow generation into and out of cell i from neighbouring cell j, from time $N-1$ to N respectively.

In order to calculate the volumetric balance, initial conditions of each streamflow component of the streamwater must be known in each cell. The components of flow are defined as a fraction of the total volume (V_i) such that:

$$\sum_{k=1}^{K} f_{i(k)}^N = \frac{\sum_{k=1}^{K} V_{i(k)}^N}{V_i^N} = 1 \tag{7}$$

where $f_{i(k)}{}^N$ [L^3/L^3] is defined as the kth fraction of each streamflow component.

If the form of the function of fluxes can be reconstructed from the flow solution then, using the modified mixing-cell approach of Campana and Simpson (1984), each component of streamflow can be determined by substituting (6) into (7) and rearranging giving:

$$\sum_{k=1}^{K} f_{i(k)}^N = \frac{\sum_{k=1}^{K}\left(V_{i(k)}^{N-1} + \sum_{j=1}^{n} V_{ji(k)}\Big|_{N-1}^{N} - \sum_{j=1}^{m} V_{ij(k)}\Big|_{N-1}^{N}\right)}{V_i^N} \tag{8}$$

Considering only the kth fraction and expanding out the volumetric terms to explicitly represent the fractions, then rearranging yields:

$$f_{i(k)}^N = \left(\frac{V_i^{N-1}}{V_i^N} - \frac{\sum_{j=1}^{m} V_{ij}\Big|_{N-1}^{N}}{V_i^N}\right) f_{i(k)}^{N-1} + \frac{\sum_{j=1}^{n} V_{ji}\Big|_{N-1}^{N} f_{j(k)}^{N-1}}{V_i^N} \tag{9}$$

where there are n sources and m sinks for cell i; $f_{j(k)}^{N-1}$ denotes fraction k at time $N-1$ in neighbouring cell j. The terms on the right hand side of equation (9) relate to the stability of this approach. They can be considered from left to right as a) the ratio of storage in the previous time step to the current storage less the ratio of outflow volume to storage and b) the ratio of inflow volume to storage. The stability of this method requires that the volume of water entering or leaving the stream cell over a time step is not greater than the storage at the end of the time step. This is fairly intuitive as it is not possible to remove more mass than existed at the start of the time step $(N-1)$ or insert more mass than exists at the end of the time step (N). For each component of streamflow the fraction is determined using the modified mixing cell which approaches a perfectly mixed cell as the time step approaches zero. A perfectly mixed cell will completely mix all contents across the entire cell instantaneously and takes the form:

$$f_{i(k)}^N = \frac{V_i^{N-1}}{V_i^N} f_{i(k)}^{N-1} - \frac{\sum_{j=1}^{m} V_{ij}\Big|_{N-1}^{N}\left(f_{i(k)}^{N-1} + \sum_{j=1}^{n} V_{ji}\Big|_{N-1}^{N} f_{j(k)}^{N-1}\right)}{V_i^N + \sum_{j=1}^{n} V_{ji}\Big|_{N-1}^{N}} + \frac{\sum_{j=1}^{n} V_{ji}\Big|_{N-1}^{N} f_{j(k)}^{N-1}}{V_i^N} \tag{10}$$

It can be readily seen that equation (9) approaches equation (10) as the time step approaches zero, as only the first term on the right hand side in both equations will remain.

In applying this method, volumes in and out need to be determined at the start and end of each time step. This requires reconstruction of the functions describing flux in and out of each cell. The approach used in calculating volumes needs to be consistent with the manner in which the fluid mass balance is calculated in the particular model used. In this study, the HydroGeoSphere (HGS) (Therrien et al., 2009) code is used in which the flux Q between two adjacent nodes is back calculated at the end of the time step, giving rise to the following equation for evaluating the volume in or out over each time step:

$$V_{ij}^N = Q_{ij}^N \times \Delta t^N \quad \text{where } \Delta t^N = \left(t^N - t^{N-1}\right) \tag{11}$$

where Q_{ij}^N denotes the calculated flux from HGS from node i to j over Δt.

The form of equation (11) will vary from code to code depending on how the fluid mass balance is calculated. Furthermore, the

choice of numerical approach, be it finite difference, finite volume or finite element, is irrelevant as long as the volumetric balance for each cell is formulated correctly and is mass conservative. The latter requirement is due to the error in the mass balance at each time step being cumulative in the HMC method. Stability of the HMC method is not guaranteed for any flow solution as highlighted above. The use of suitable convergence criteria within the flow solution is imperative in successful application of the HMC method. A strict convergence criterion that is applied at the nodal level is required. The nodal flow check tolerance in HGS, which is derived in McLaren et al. (2000), was utilised to ensure the nodal volumetric balances calculated in the HMC method were sufficient in preventing large cumulative errors. The choice of time step and cell size also plays an important role in the stability of the HMC method because the volumetric balance at each HMC over each time step is directly related to time step and cell size. The proportion of volumes of water entering or leaving each cell over each time step compared to the storage volume in the cell has a direct impact on the HMC method's stability. The use of small HMCs and large time steps can lead to the volume entering or leaving a cell being greater than the storage and as such the method will become unstable causing spurious oscillations. Hence it is necessary to use suitable time steps for a fixed grid (i.e. fixed cell size) to ensure stability.

3.2. Implementation of the HMC method in HydroGeoSphere

The testing of the HMC method outlined in this paper was carried out by considering two conceptual test cases using the HGS model. HGS solves the diffusion wave approximation to the 2D Saint Venant equations in the surface domain and solves a modified form of the 3D Richards equation for variably saturated flow in the subsurface domain using a control volume finite element approach (details of the model can be found in Therrien et al. (2009)). The surface and subsurface are coupled using either continuity of head or (as in this study) a conductance concept, with exchanges between the two domains given by:

$$q_{\text{exch}} = \frac{k_{\text{r}} K_{zz}}{l_{\text{exch}}}(h_{\text{o}} - h_{\text{pm}}) \tag{12}$$

where q_{exch} [L/T] is the exchange flux between the surface and subsurface domain; k_{r} [dimensionless] is the relative permeability; K_{zz} [L/T] is the saturated hydraulic conductivity of the porous medium; l_{exch} [L] is the coupling length, h_{o} [L] and h_{pm} [L] are the heads of the surface and subsurface, respectively. HGS has been verified for both gaining (Therrien et al., 2009), losing and losing disconnected streams (Brunner et al., 2009a,b). The model solves the governing flow equations using the finite element (FE) method, finite volume (FV) method or, alternatively, the finite difference (FD) method applied on a node centred grid (Therrien et al., 2009).

Application of the HMC method requires specific HGS model outputs in order to accurately construct the volumetric balances in each HMC. As HGS utilises a node centred approach, the following HGS outputs are required for the volumetric balance at any given node:

1) Computed surface water depth at the node – for the storage at each time step.
2) Contributing area, (CA [L^2]) for the node determined from finite element basis functions (1/4 of the area of each element adjacent to the node for both FD and FE on a structured rectangular grid) – for the Storage (=depth × CA) [L^3] at each time step.
3) Exchange flux between the subsurface and surface node – for the volume (Eq. (11)) exchanged between the subsurface and surface over each time step.
4) Flux from upstream contributing nodes – for the upstream volume (Eq. (11)).
5) Flux to downstream nodes – for the downstream volume (Eq. (11)).

1) and 2) are used to calculate V_i, 3) used to calculate V_{ji} for the exchange, 4) used to calculate V_{ji} for upstream flow, 5) used to calculate V_{ij} for downstream flow. The initial values for the fractions of streamflow are subjective and so a dummy (or undefined) fraction can be used until the streamwater is turned over at which point the dummy fraction will be zero.

This output data provides all the information required to apply the HMC method and determine the groundwater component of streamflow at each time step in each cell of the stream. The partitioning of groundwater, overland flow and rainfall entering the HMC is calculated from the upstream cell in the previous time step. The fractions of streamflow components leaving a given cell over a given time step are given by the cells' fractions at the previous time step. In doing so, water entering over a given time step remains in the given cell until the next time step. The HMC method was coded in Visual Basic for Excel and is used as a post-processing tool on HGS outputs.

3.3. Verification of mass conservation in the HMC method

3.3.1. Test case 1

This test case is used to check that the flow components can be tracked accurately and to explore the significance of grid discretisation. The surface domain of the model is subjected to groundwater discharge (gaining conditions) across half of the model surface. This groundwater discharge in the gaining region is equal to the summed exfiltration obtained from the overall water balance, providing a benchmark against which the method can be tested.

The model domain is 2 m × 1 m × 1 m, split into two evenly sized rectangular cells (Fig. 4). Two regions are highlighted in Fig. 4, a gaining region in one half and a non-gaining region in the other. The non-gaining region has negligible interaction with the subsurface. With the soil fully saturated and an initial surface water depth of 0.01 m across the surface domain, a square pulse of groundwater (1.0 m^3/day for 0.1 days) is injected into the subsurface cell underlying the gaining region. No-flow boundaries are applied to all edges of the model domain allowing the groundwater pulse to be the only forcing function within the model. This simulation is run over a period of half a day with the groundwater pulse applied at 0.1 days. The grid spacing is 1 m along the x, y and z axes. For this HGS simulation, a control volume finite difference formulation is used to solve the coupled surface and subsurface flow equations. The nodal properties give rise to three 'cells' for the HMC method (see Fig. 4). Note that rather than considering six nodes individually, the HMCs each consist of 2 adjacent nodes perpendicular to the flow direction. The HMCs are given the initial conditions of containing 'surface water' only and hence $f_{\text{SW}} = 1$ and $f_{\text{GW}} = 0$ for all HMCs at $t = 0$.

In the surface domain, a high value of Manning's n (1.5×10^{-5} day/$m^{1/3}$) is used in order to make the transient part of the simulation apparent. The aquifer parameters are defined such that surface/subsurface interactions other than the groundwater pulse are negligible. The porosity is 0.45 and a low value of hydraulic conductivity (1×10^{-4} m/day) is used to effectively render the subsurface inactive with regard to infiltration. As the subsurface is fully saturated, infiltration is negligible, and the groundwater injected to the system will directly result in a fluid flux from the subsurface to the surface domain. The coupling length chosen (1×10^{-5} m) is sufficiently small to achieve continuity of

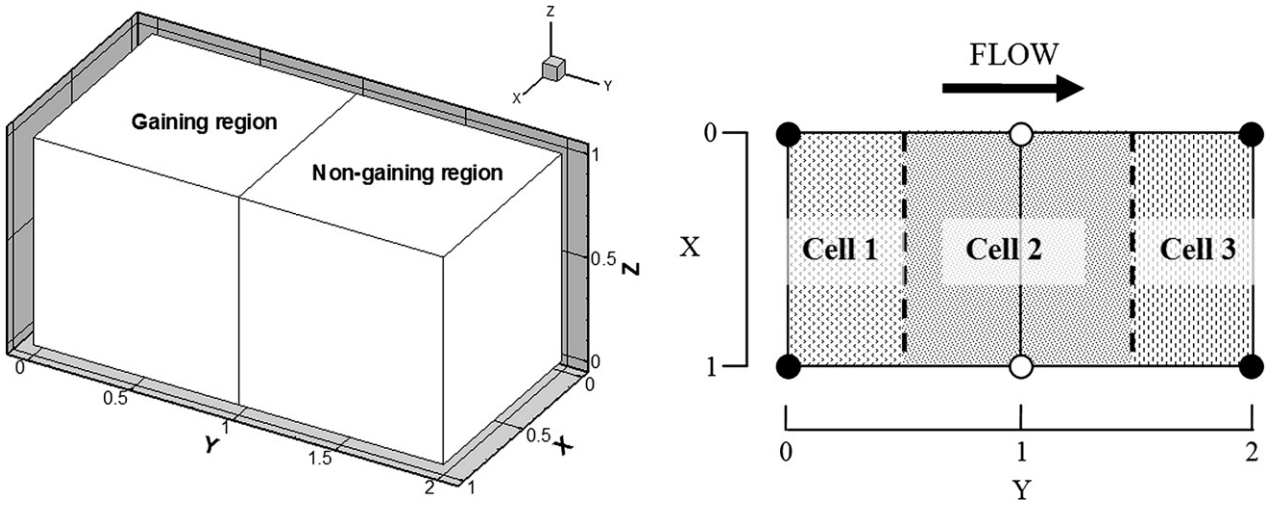

Fig. 4. Test case 1: "two-region" model grid, and HMCs for HGS nodes in "two-region" model grid. In the right part of the figure the two nodes at $y = 0$ belong to HMC 1, the two nodes at $y = 1$ belong to HMC 2 and the nodes at $y = 2$ belong to HMC 3.

head between the surface and subsurface. A maximum time step of 1×10^{-3} days was used for the first simulations. As the diffusion wave approximation to the Saint Venant Equations is used in HGS, inertial effects are ignored and therefore water entering the gaining region will move to the non-gaining region and not flow back as it would if inertial effects were included.

Fig. 5 shows the volumetric balances of surface water and groundwater calculated for each of the three HMCs in the model, highlighting the subtle complexities that can easily be overlooked when considering the dynamics of such a system. It can be seen in cell 1 of Fig. 5 that whilst the groundwater pulse is applied to the subsurface, groundwater is entering the gaining region, causing an increase in volume (and hence head) and a resultant flux from the gaining to the non-gaining region. Moreover, the volume of surface water in the gaining region decreases as the groundwater enters, which is due to the water in the gaining region flowing to the non-

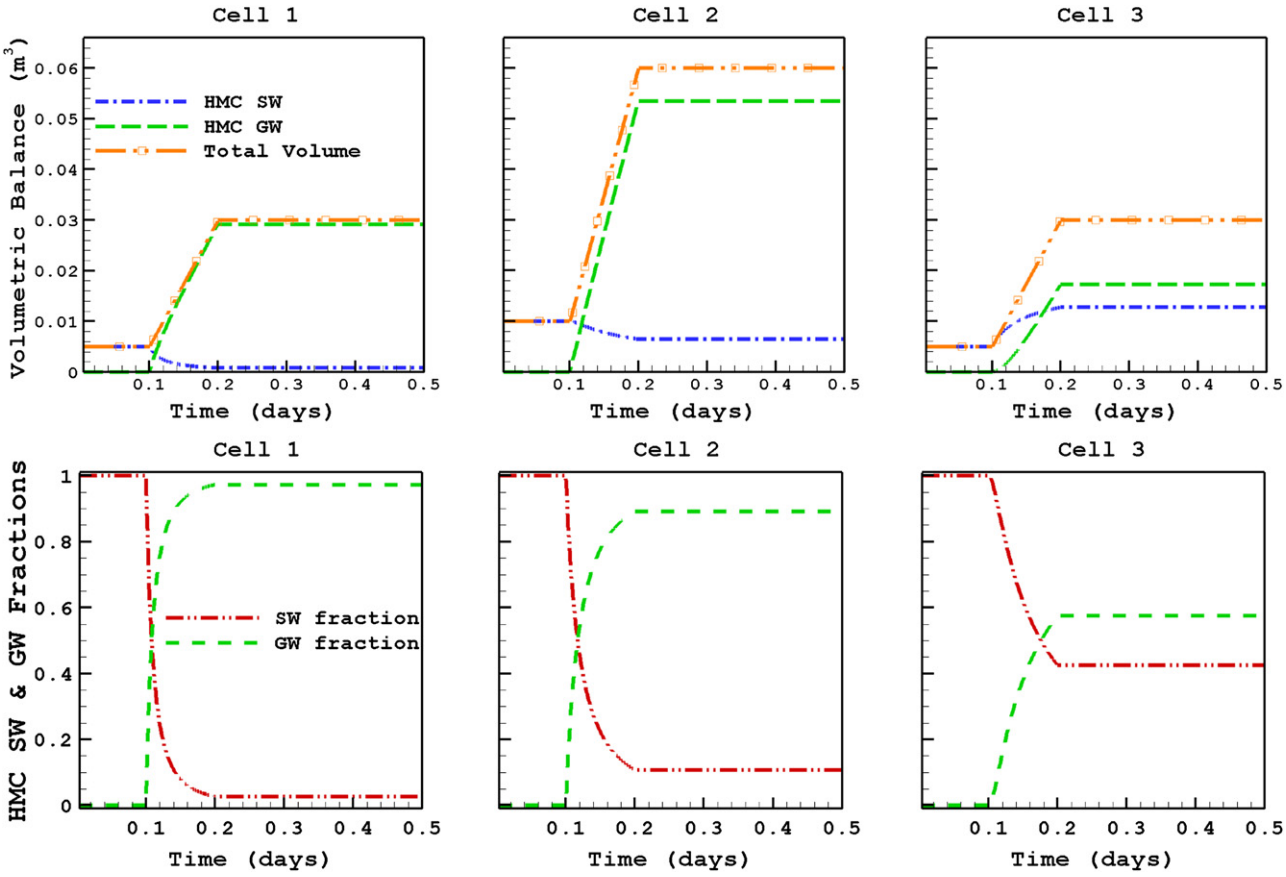

Fig. 5. HMC, SW and GW balances (top panel) and fractions (bottom panel) for test case 1. The volumetric balance in the top row shows the HMC calculated balances for SW and GW in the HMCs as well as the total volume in the cell which is calculated directly from the model outputs. The HMC SW and GW fractions in the bottom panel are calculated independently of each other.

gaining region. The volumes of groundwater and surface water in cell 2 are collectively larger than those in cells 1 or 3 because the contributing area of cell 2 is twice that of cells 1 and 3 (see Fig. 4). The small lag between the surface water and groundwater curves in the volumetric balance for cell 3 (Fig. 5) indicates that surface water initially contributes more to the flow from the gaining region to the non-gaining region, as the surface water is displaced by the groundwater. The SW and GW balances for each of the HMCs in the top panel of Fig. 5 are also shown with the total cell volume. Clearly, the SW and GW balances sum to the total volume, indicating that that the HMC method conserves mass. The SW and GW fractions for each of the HMCs in the bottom panel of Fig. 5 are seen from the average of the two fractions to be inversely proportional to each other, as expected. As the balances are calculated independently, this further highlights the accuracy within the HMC method.

The relative error (ϵ) in the balances is based on Eq. (7) and is determined using the following equation:

$$\epsilon = \left| 1 - \sum_{j=1}^{k} f_{i(k)}^{N} \right| \tag{13}$$

The relative error relates to the accuracy of the numerical methods for solving the flow equations, which is determined by the convergence criteria used in the numerical model. This error grows slightly due to round-off errors and imperfect balances in the numerical scheme used to solve the flow equations (finite difference in this case). Such imperfect balances will always exist due to error in the numerical scheme adopted, however they can be minimised by use of a small value for the convergence criterion. In this test case the maximum relative error in the HMC method was 1.5×10^{-3}% in cell 1.

It is clear from the balances in Fig. 5 that the changes in the SW and GW volumes and fractions are rapid, and that all changes occur within the timeframe of the groundwater pulse that is applied. The spatial and temporal discretisations used in the HGS model determine the resolution seen in the outputs, and they play a key role in the HMC method solution. It is therefore necessary to elucidate to what extent the maximum relative error in the HMC solution depends on discretisation. To investigate the effect of discretisation, the grid spacing dy in the flow direction (y axis) is reduced in HGS from 1 m to 10 cm. As a result, the number of corresponding cells in the HMC method increases to 21 (see Fig. 6). Three different simulations are then run to test the impact of time discretisation, with constant time steps equal to 10^{-2}, 10^{-3} and 10^{-4} days, respectively.

The effects of temporal discretisation on the SW and GW fractions for the case of d$y = 10$ cm are shown in Fig. 7. In Fig. 7, only the two end cells (1 and 21) and the middle cell (11) are shown. It can be seen that the finer time steps make little difference to the SW and GW fractions in cells 1 and 11, but that a distinctly different solution of the SW and GW fractions arises in cell 21 for the three time steps used, with convergence at $t = 10^{-3}$ and 10^{-4} days. It follows that it is important to note that the time step used in the model will dictate the SW and GW fraction profiles in the HMC method. As highlighted in the theory, as dt approaches zero, a perfectly mixed cell solution is approached. Variations in grid size change the representative area of the HMCs. For example, halving the grid size would result in the HMC area for the larger grid size being represented by two HMCs for the halved grid size. As the HMCs are representative of an area and not a point, results based on different grid discretisations are not directly comparable. However, finer grids will give greater spatial resolution of the SW and GW fractions along the surface. It follows that smaller cell sizes in the model grid and hence in the HMC method, result in greater spatial clarity of the solution, converging towards a point solution as dy approaches zero. As dy approaches zero, the area of the cell approaches zero and hence the volume in the cell approaches zero. Given that stability requires that the volume in or out of the cell cannot be greater than the storage, the time step dt will also have to decrease as dy decreases to ensure numerical stability.

A second approach to testing the accuracy of the HMC method is to compare the total volumes of surface water and groundwater resulting from summing these components in each HMC at the end of the simulation with the overall water balance in the model. By summing the final volumes of groundwater in each HMC, and comparing these to the total volume that was exchanged from the subsurface to the surface domain during the simulation, a global volume error (GVE) can be defined as follows:

$$\text{GVE}\ (\%) = \left| 1 - \frac{\sum_{\forall i} f_{i(\text{GW})}^{N} V_i^{N}}{\sum_{\forall N} Q_{\text{SE}}^{N} \Delta t^{N}} \right| \times 100 \tag{14}$$

where Q_{SE}^{N} [L^3/T] is the summed exfiltration across the model domain at time N from the overall water balance of HGS.

This measure gives the error of the HMC method relative to the summed exfiltration from the overall water balance. The cumulative error of the HMC method (as opposed to the instantaneous nodal fluid mass balance error in HGS) will grow according to the convergence criteria, number of time steps and number of stream

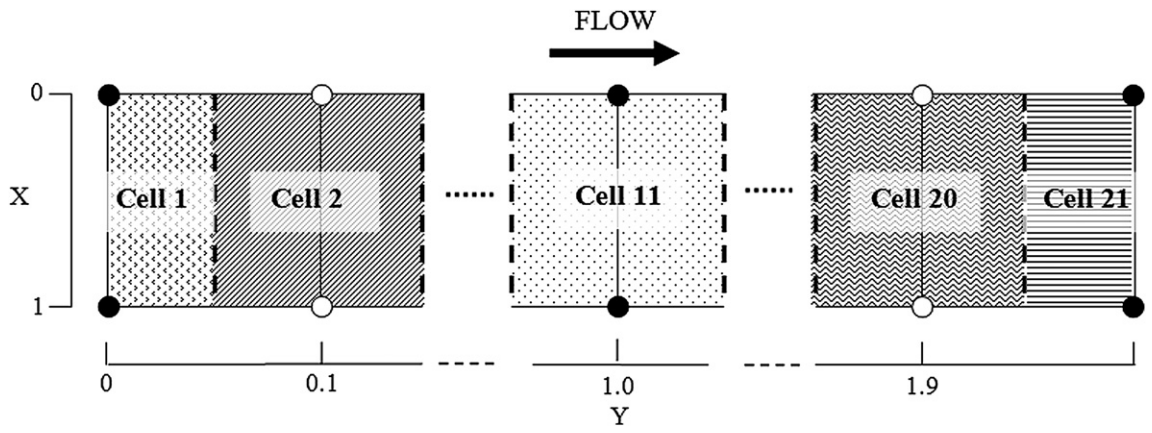

Fig. 6. The 21 HMCs for the "two-region" model with d$y = 10$ cm.

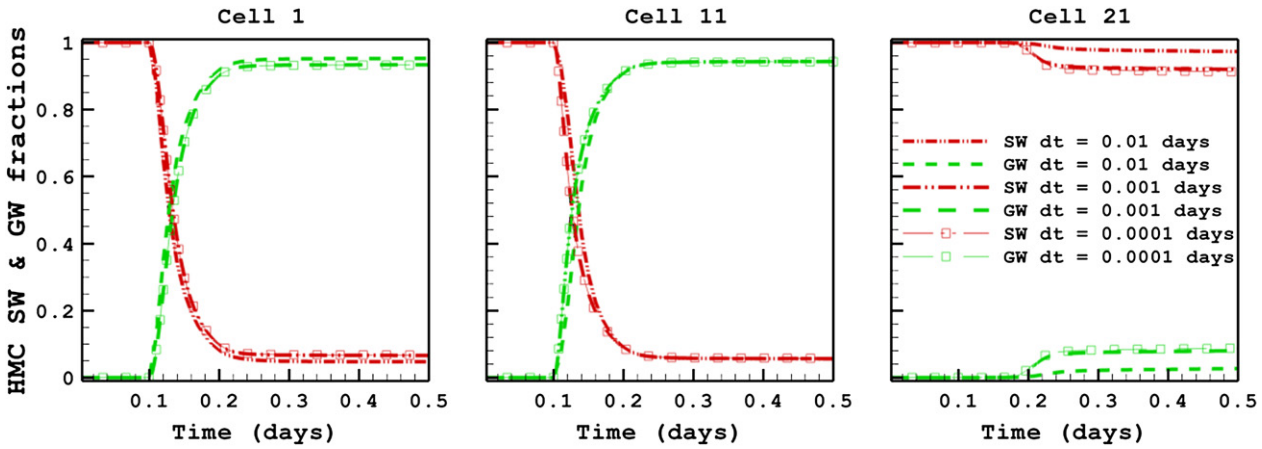

Fig. 7. Effect of temporal discretisation on the SW and GW fractions in HMCs 1, 11 and 21.

cells. As the GVE is based on the summed exfiltration from the overall water balance, it can only be used along completely gaining sections. It also requires that all water is retained in the model domain (i.e. no losses). The maximum relative error and GVE are given in Table 1 for the different spatial and temporal discretisations tested, highlighting both the reduced maximum relative error and GVE as the spatial and temporal resolution is increased.

In the HMCs of Test case 1, the relative and absolute errors are relatively small and consequently the HMC method can be used in larger and more complex model scenarios provided that fluid mass conservation is fulfilled.

3.3.2. Test case 2

The model setup for Test case 2 mirrors the physical processes of the catchment shown in Fig. 1. This test case is used to test not only the effects of time lags (seen in the hydrographs of Fig. 2) and accurate attribution and tracking of streamflow generation mechanisms, but also to test the HMC method in a highly transient model scenario whilst comparing the HMC method's groundwater component of streamflow with the summed exfiltration from the overall water balance of the model.

Test case 2 is loosely based on the tilted V-catchment by Panday and Huyakorn (2004), which has been used in verification of surface/subsurface interaction in fully integrated models such as MODHMS and HGS. A number of modifications are carried out to the V-catchment to mirror the spatial and temporal distribution of the catchment shown in Fig. 1. In order to distribute the subsurface to surface exchange to the stream over its entire length, the slopes are reduced, resulting in a significantly flatter catchment. The model domain is 1000 m along the y axis by 810 m along the x axis (catchment area of 810,000 m^2), with a homogeneous soil layer thickness of 20 m at ($x = 800$–810 m, $y = 0$ m) increasing in thickness with a gentle surface slope of 5×10^{-4} m/m along the y axis (from $y = 0$ m to $y = 1000$ m) and 0.02 m/m along the x axis (from $x = 800$ m to $x = 0$ m) (Fig. 8). With the use of the gentle slopes, the head gradient required in order to produce an exchange from the subsurface to the surface along the entire stream is achieved by raising the adjacent plane 2 m over a 5 m length above the streambed as shown in the cross section of Fig. 9.

Grid spacing along the x axis is 50 m from $x = 0$ to 750 m, 25 m from $x = 750$ to 775 m, 15 m from $x = 775$ to 790 m, 5 m from $x = 790$ to 800 and 10 m from $x = 800$ to 810 m. The grid spacing is 50 m along the y axis and 1 m along the z axis for the first 10 m below the surface with a thickness of 10–26.5 m, varying with the slopes of the catchment for the bottom layer. Streamflow at the downstream boundary is governed by a critical depth boundary condition at the end of the stream, which acts at nodes (800,0,0) and (810,0,0). The critical depth boundary in HGS specifies the surface head to be at critical depth at the nodes which are set with this boundary condition.

Saturation–relative permeability and saturation–pressure relationships are described by the Van Genuchten (1980) equations. The soil is a homogeneous sand with the soil parameters derived from Carsel and Parrish (1988). The surface friction is described using Manning's n, with a value representing a straight uniform channel (Chow, 1959), and a rill storage height and obstruction height (as defined in Panday and Huyakorn (2004)) of 1 mm and 0 mm, respectively. The rill storage height provides a threshold to surface flow whilst the obstruction height provides retardation to flow. The surface and subsurface parameters are detailed in Table 2. The coupling length (equation (12)) is chosen such that continuity of pressure at the surface/subsurface interface is maintained, without jeopardising the accuracy of the flow solution. The solution of continuous pressure at the surface/subsurface interface leads to much larger run times for the simulations in this study (see Ebel et al., 2009), however for small coupling lengths, the solution approaches that of continuous pressure at the surface/subsurface interface.

The simulations for the hypothetical catchment are carried out in two phases:

1. Firstly, initial conditions are generated by running the model with a fully saturated subsurface with only the critical depth forcing function in the surface domain for approximately 40 days. This first simulation provides quasi steady-state initial conditions for phase 2.
2. Based on these initial conditions the model is run for another 40 days with 3 rainfall events and constant groundwater pumping throughout the entire simulation. The drawdown around the pump results in a losing section along a part of the stream. Rainfall is applied across the entire catchment, starting at time $t = 0$ s at a rate of 5.88×10^{-7} m/s (2.12 mm/h) for a day

Table 1
Maximum relative error in the HMC method, and the global volume error (GVE) for the HMC method.

	HMC max. relative error	GVE	Time steps
$dy = 1$ m, $t = 0.001$ days	1.5×10^{-3}%	1.97×10^{-4}%	500
$dy = 10$ cm, $t = 0.01$ days	1.8×10^{-4}%	5.23×10^{-10}%	50
$dy = 10$ cm, $t = 0.001$ days	3.6×10^{-5}%	1.17×10^{-10}%	500
$dy = 10$ cm, $t = 0.0001$ days	3.9×10^{-7}%	2.81×10^{-11}%	5000

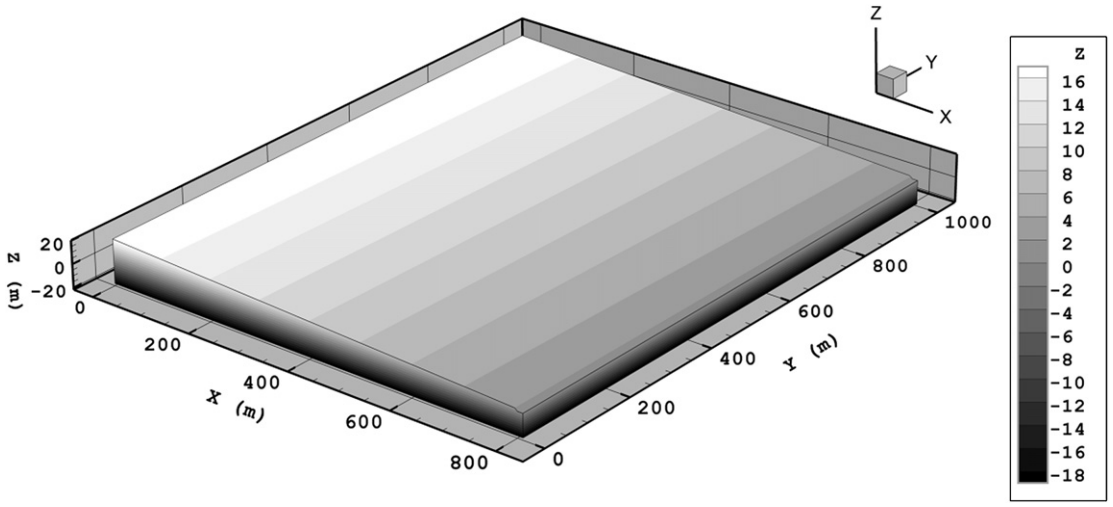

Fig. 8. Test case 2 catchment model (modified version of the V-catchment in Panday and Huyakorn (2004)). The contours correspond to the elevation.

at a time with three recovery periods after each rainfall period of 10, 5 and 22 days, respectively for each rainfall event. Pumping is applied at node (750,500,0) at a rate of -0.02 m^3/s throughout the simulation time. This extraction rate is sufficient to produce losses over part of the stream. Over the length of the simulation there is a rainfall input of 1.75×10^5 m^3 and a loss through pumping of 6.84×10^4 m^3. The maximum time step used in the second phase of the simulation is 100 s. The rainfall and pumping in the second phase create highly transient conditions. The length of the stream that is losing is changing throughout the simulation. The nature of this transience in the streamflow conditions allows for rigorous stability testing of the HMC method because the stream cells are switching between gaining and losing and are subject to sharp changes in volume and rate of change of volume in the cell.

The rainfall events in the simulations provide recharge to the groundwater system, sustaining flow to the stream. However, the gentle rainfall events and gentle slopes in the catchment result in pure recharge with no overland flow on the planes and hence no direct overland flow to the stream itself. Fig. 10 highlights the changes in the subsurface to surface exchange, as well as the depth and velocity along the stream at time = 1 s, 12 days and 40 days. At $t = 1$ s in Fig. 10, the initial stream is gaining along its entire length, before groundwater abstraction has taken effect. At $t = 12$ days, there is an increased discharge of groundwater at the top and bottom areas of the stream, which can be attributed to the recharge resulting from rainfall as well as stream losses in the middle section due to near stream groundwater extraction. The proportion of the stream that is gaining and losing is varying throughout the entire simulation.

At $t = 40$ days, the subsurface to surface exchange to the stream has decreased along the length of the stream due to the last rainfall event finishing 20 days earlier. It also shows an increased loss from the stream over the middle losing section due to reduced recharge in response to the groundwater extraction. This loss rate from the stream in the middle causes the stream depth to drop over the losing region, however streamflow is maintained through the entire simulation. This qualitative analysis provides a reasonable understanding of the governing processes in the system. For quantifying the groundwater component of streamflow, the HMC method is required.

The HMC method is applied to each pair of adjacent nodes that are located at $x = 800$ m and $x = 810$ m and that lie in the stream perpendicular to the direction of flow. HMCs are numbered from upstream ($y = 1000$ m) to downstream ($y = 0$ m) and correspond perfectly to the HGS cells. This gives rise to 21 HMCs, with 20 surface cells ($x = 800$–810 m and $y = 0$–1000 m) defined as the stream. As a node based approach is used, the contributing area of nodes lying along $x = 800$ m takes into account the surface cells lying between $x = 795$ and 800 m. The HMC maximum relative error in the simulation was 8.7×10^{-3}% in HMC 13 at around $t = 12$ days.

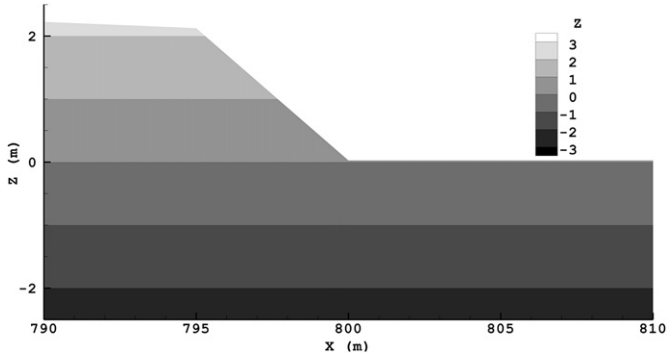

Fig. 9. Part cross section of hypothetical catchment highlighting the raised plane which is used to create a greater hydraulic gradient next to the stream leading to constant subsurface to surface exchange along the entire length (from $x = 790$ to 810 m, at $y = 0$ m and $z = -4$ to 2 m). The plane (left), bank (middle) and streambed (right) are seen in the division of top cells.

Table 2
Surface and subsurface parameters for test case 2.

Parameter	Value
Surface	
Manning's roughness	0.015 s/m$^{1/3}$
Rill storage height	0.001 m
Obstruction storage height	0.0 m
Subsurface	
Porosity	0.1
Saturated hydraulic conductivity	8.25×10^{-5} m/s
Van Genuchten α	14.5 m^{-1}
Van Genuchten β	2.68
Residual saturation θ_r	0.045
Surface/subsurface coupling	
Coupling length	0.5 m

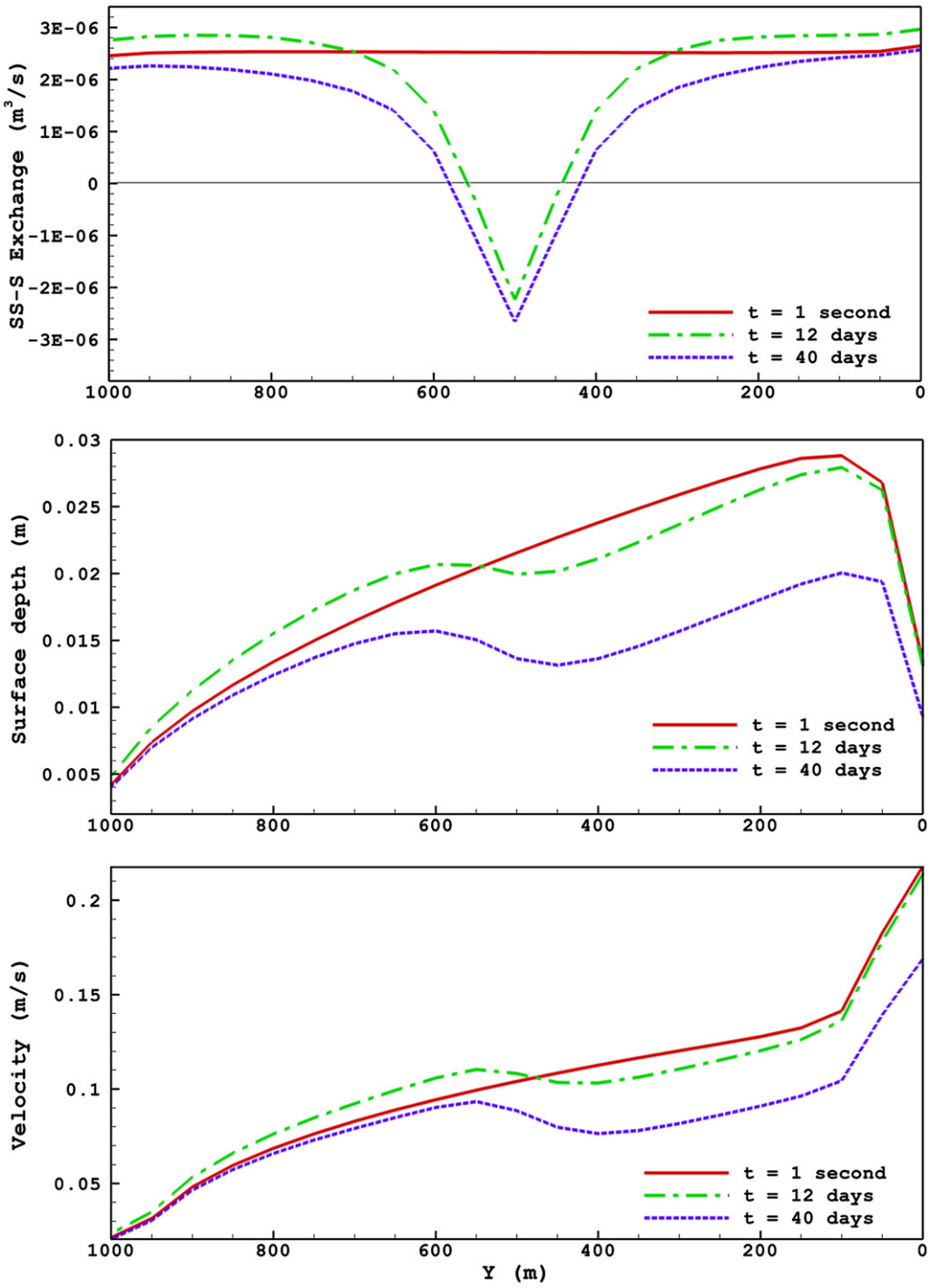

Fig. 10. Evolution of the losing section of the stream in the hypothetical catchment. A positive exchange in the top panel of plots denotes subsurface to the surface exchange and vice versa for a negative exchange. The depth and velocity profile along the stream are shown below. At $t = 1$ s, the stream is gaining along the full length. At $t = 12$ days, the pumping has reduced the positive exchange section of the stream adjacent to the pumping location. At $t = 40$ days, the stream is partially losing along a small section whilst maintaining flow along the losing section.

The use of the HMC method allows the quantification of the groundwater component of streamflow at any cell along the stream. Since the simulation setup does not produce overland flow, the streamflow in each HMC consists of the groundwater component and the direct rainfall component of streamflow. The resultant groundwater component and direct rainfall fractions before and after the first rainfall event for the HMCs located at $y = 0$, 600 and 1000 m are shown in Fig. 11. In Fig. 11a), the rise and fall of the direct rainfall fraction is sharp and fast in cell 1 and slower and longer in cells 13 and 21. This can be attributed to the time lags of upstream flow that are evident at the downstream cells and to the streamflow velocity in each cell. In Fig. 10, the streamflow velocity is seen to increase from the top of the stream ($y = 1000$ m) to the bottom of the stream ($y = 0$ m) as water keeps entering the stream, although this is only seen in the gaining regions. At $t = 12$ and 40 days, the stream is losing over the middle section which is clearly

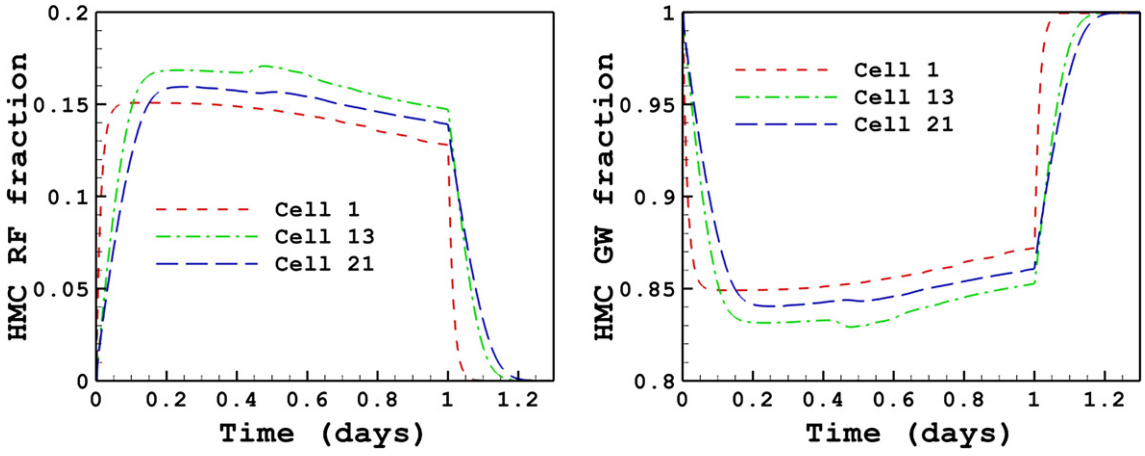

Fig. 11. HMC direct rainfall and groundwater component fractions before and after the first rainfall event for cells 1, 13, and 21. Note the time lags of rainfall in the downstream cells 13 and 21 (~3.5 h).

evident in Fig. 10 at around $y = 400$ m where the velocity drops off only to start increasing again at $y = 500$ m. As surface flow velocity is faster at the bottom sections of the catchment, storage effects alone can be ruled out as causing the slower recession of the rainfall fraction in cells 13 and 21. The rainfall fraction after the first rainfall event ($t = 1$ day) in cells 13 and 21 must be due to rainfall from upstream cells in which there is a significant time lag of approximately 0.2 days. It is also apparent that the rainfall fraction in cell 13 is greater than the fraction in cell 21, which can be attributed to the increase in the groundwater entering when moving downstream of cell 13. As there are only two streamflow generation mechanisms in this simulation, the same explanation leads to the groundwater component of streamflow results shown in Fig. 11b).

The resulting partition of the groundwater component of streamflow is shown in Fig. 12. The HMC groundwater component of streamflow and direct rainfall to the stream are calculated using the HMC fractions in HMC 21. It is highlighted that the summed exfiltration from the overall water balance cannot be used as a measure of the groundwater component of streamflow as it clearly leads to an overestimation as the summed exfiltration is greater than the streamflow. This is due to the losses occurring in the middle section of the stream, which is not captured by the summed exfiltration upstream of this section where flows are partially lost through the losing section of the stream. The infiltration in the overall water balance cannot be utilised to account for the net change either, due to the very large amount of infiltration over the planes resulting from the rainfall events. Whilst the error in the groundwater component of streamflow as estimated using the summed exfiltration along the stream may appear small, the volumetric differences found by integrating the summed

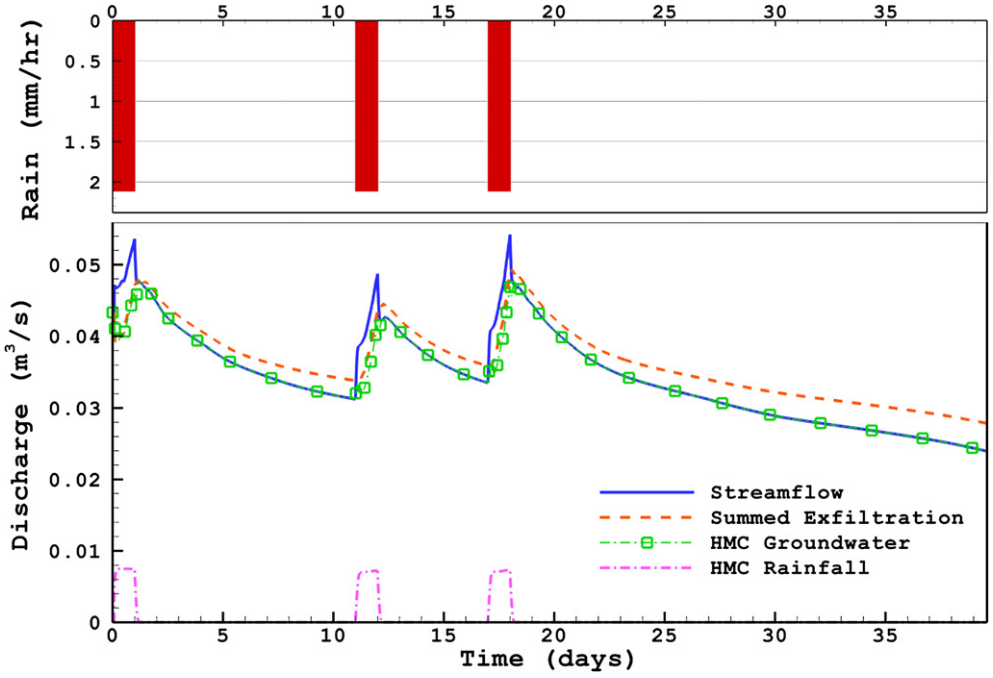

Fig. 12. Hyetograph for catchment and Hydrograph at the catchment outlet, showing separation of direct rainfall and groundwater components of streamflow, as well as the summed exfiltration from the overall water balance. The summed exfiltration (SE) from the water balance is clearly seen to exceed the outflow in this hypothetical catchment. The HMC direct precipitation and groundwater components of streamflow are calculated using the HMC fractions in HMC 21.

exfiltration and HMC groundwater component of streamflow over the recession periods ($t = 1–11$ days, $t = 12–17$ days and $t = 18–40$ days) were found to be 1620 m^3 (1.62 ML), 858 m^3 (0.85 ML) and 5420 m^3 (5.42 ML), respectively. This is a total of 7340 m^3 (7.34 ML) during the recession periods, a significant difference in response to a single hydrograph event in a small catchment. Given the area of this catchment (0.81 km^2), the impacts on the difference/error that would be seen in a larger catchment are significantly greater. However, it is not only the area of the catchment that will make use of the HMC method critical in determining the groundwater component of streamflow generation. The travel time within the streams also undermines the application of the summed exfiltration as seen in Fig. 11. As the streams become longer, the streamflow travel time from upstream to downstream increases, and as such the summed exfiltration can be much sharper and completely out of phase with the total streamflow as hypothesised in Fig. 2. The proportion and distribution of both gaining and losing sections also have a clear effect of leading to overestimation of the groundwater component of streamflow at the outlet.

4. Discussion and conclusions

The hydraulic mixing-cell (HMC) method developed in this paper overcomes many of the limitations that exist in current methods of quantifying streamflow generation mechanisms based on fully integrated spatially distributed SW–GW interaction models. The HMC method accurately extracts streamflow generation mechanisms using only hydraulic information. Streamflow generation mechanisms at every HMC along the stream are extracted by post-processing of the flow solution obtained from the numerical flow model. Because the HMC method tracks the streamflow generation mechanisms along the stream, temporal and spatial components that affect these mechanisms can be accounted for. The HMC method correctly handles changing flow regimes (e.g. if a stream changes from gaining to losing within the catchment), accounts for storage effects within the channel and the time lags that occur within a catchment. These attributes give the HMC method the ability to deal with the dynamic nature of varying flow regimes in large and complex systems, such as the catchment described in Fig. 1. The only data requirements for the HMC method are the fluxes at each cell and surface water depths, which are part of the flow solution. By using this method, one does not have to make the commonly made assumptions of negligible time lags in streamflow and exchanges being always positive to the stream, in order to determine the streamflow generation mechanisms.

In the current formulation, the HMC method is based on the modified mixing cell (Campana and Simpson, 1984). Unless the mixing processes in the river are explicitly simulated, the modified mixing rule has to be used. As highlighted in the theory section, the HMC method is stable as long as the ratio of the volume of water entering or leaving an HMC to the storage volume of the HMC is less than unity. The assumption of constant river width and flow direction are used in the coding of the HMC algorithm in this study. The initial formulation of the HMC method presented here is based on the assumption of a constant river width. In models such as HGS, the width of the stream can change in response to a changing flowrate. In order to capture a changing river, the definition of the river in the HMC algorithm must match the changes in the river. Further development of the method is required to quantify streamflow generation mechanisms in such systems. The HMC method presented is applicable (in principle) to any spatially distributed flow modelling code, however the coding requires generalisation to time varying river widths and lengths. The HMC method should be routinely employed as either a subroutine within the model code or as a post-processing tool.

Acknowledgements

This work is supported by the Australian Research Council through its Linkage scheme and the South Australian Department of Water, Land and Biodiversity Conservation as industry partners under grant LP0668808. Parts of this research were funded by the Swiss National Foundation, Ambizione grant PZ00P2_126415. The views expressed in this paper are solely those of the authors.

References

Adar, E.M., Neuman, S.P., Woolhiser, D.A., 1988. Estimation of spatial recharge distribution using environmental isotopes and hydrochemical data .1. Mathematical-model and application to synthetic data. J. Hydrol. 97, 251–277.

Brunner, P., Cook, P.G., Simmons, C.T., 2009a. Hydrogeologic controls on disconnection between surface water and groundwater. Water Resour. Res. 45, W01422. doi:10.1029/2008WR006953.

Brunner, P., Simmons, C.T., Cook, P.G., 2009b. Spatial and temporal aspects of the transition from connection to disconnection between rivers, lakes and groundwater. J. Hydrol. 376, 159–169. doi:10.1016/j.jhydrol.2009.07.023.

Campana, M.E., Simpson, E.S., 1984. Groundwater residence times and recharge rates using a discrete-state compartment model and C-14 data. J. Hydrol. 72, 171–185.

Carsel, R.F., Parrish, R.S., 1988. Developing joint probability-distributions of soil-water retention characteristics. Water Resour. Res. 24, 755–769.

Chapman, T.G., 2003. Modelling stream recession flows. Environ. Model. Softw. 18, 683–692.

Cheng, J.R.C., Hunter, R.M., Cheng, H.P., Richards, D.R., 2005. A parallel software development for watershed simulations. Computational Science - Iccs 2005, Pt 1, Proceedings 3514, 460–468.

Chow, V.T., 1959. Open Channel Hydraulics. McGraw-Hill, New York.

Croton, J.T., Barry, D.A., 2001. WEC-C: a distributed, deterministic catchment model – theory, formulation and testing. Environ. Model. Softw. 16, 583–599.

Ebel, B.A., Mirus, B.B., Heppner, C.S., VanderKwaak, J.E., Loague, K., 2009. First-order exchange coefficient coupling for simulating surface water–groundwater interactions: parameter sensitivity and consistency with a physics-based approach. Hydrol. Process. 23, 1949–1959.

Eckhardt, K., 2008. A comparison of baseflow indices, which were calculated with seven different baseflow separation methods. J. Hydrol. 352, 168–173.

Facchi, A., Ortuani, B., Maggi, D., Gandolfi, C., 2004. Coupled SVAT–groundwater model for water resources simulation in irrigated alluvial plains. Environ. Model. Softw. 19, 1053–1063.

Gilfedder, M., Walker, G.R., Dawes, W.R., Stenson, M.P., 2009. Prioritisation approach for estimating the biophysical impacts of land-use change on stream flow and salt export at a catchment scale. Environ. Model. Softw. 24, 262–269.

Hattermann, F., Krysanova, V., Wechsung, F., Wattenbach, M., 2004. Integrating groundwater dynamics in regional hydrological modelling. Environ. Model. Softw. 19, 1039–1051.

Hewlett, J.D., Troendle, C.A., 1975. Non-point and diffuse water sources: a variable source area problem. In: Watershed Management. Am. Soc. of Civil Eng., New York, pp. 21–46.

Jones, J.P., Sudicky, E.A., Brookfield, A.E., Park, Y.J., 2006. An assessment of the tracer-based approach to quantifying groundwater contributions to streamflow. Water Resour. Res. 42.

Kollet, S.J., Maxwell, R.M., 2006. Integrated surface–groundwater flow modeling: a free-surface overland flow boundary condition in a parallel groundwater flow model. Adv. Water Resour. 29, 945–958.

McCallum, J.L., Cook, P.G., Brunner, P., Berhane, D., 2010. Solute dynamics during bank storage flows and implications for chemical base flow seperation. Water Resour. Res. 46, W07541. doi:10.1029/2009WR008539.

McGlynn, B.L., McDonnell, J.J., 2003. Quantifying the relative contributions of riparian and hillslope zones to catchment runoff. Water Resour. Res. 39.

McGuire, K.J., McDonnell, J.J., 2006. A review and evaluation of catchment transit time modeling. J. Hydrol. 330, 543–563.

McLaren, R.G., Forsyth, P.A., Sudicky, E.A., VanderKwaak, J.E., Schwartz, F.W., Kessler, J.H., 2000. Flow and transport in fractured tuff at Yucca Mountain: numerical experiments on fast preferential flow mechanisms. J. Contam. Hydrol. 43, 211–238.

Mirus, B.B., Loague, K., VanderKwaak, J.E., Kampf, S.K., Burges, S.J., 2009. A hypothetical reality of Tarrawarra-like hydrologic response. Hydrol. Process. 23, 1093–1103.

Panday, S., Huyakorn, P.S., 2004. A fully coupled physically-based spatially-distributed model for evaluating surface/subsurface flow. Adv. Water Resour. 27, 361–382.

Sayama, T., McDonnell, J.J., 2009. A new time–space accounting scheme to predict stream water residence time and hydrograph source components at the watershed scale. Water Resour. Res. 45.

Sklash, M.G., Farvolden, R.N., 1979. Role of groundwater in storm runoff. J. Hydrol. 43, 45–65.

Sophocleous, M., 2002. Interactions between groundwater and surface water: the state of the science. Hydrogeol. J. 10, 52–67.

Therrien, R., McLaren, R.G., Sudicky, E.A., Panday, S., 2009. HydroGeoSphere. A Three-dimensional Numerical Model Describing Fully-integrated Subsurface and Surface Flow and Solute Transport (Manual). Groundwater Simulations Group, University of Waterloo.

Van Genuchten, M.T., 1980. A closed-form equation for predicting the hydraulic conductivity of unsaturated soils. Soil Sci. Soc. Am. J 44, 892–898.

VanderKwaak, J.E., Loague, K., 2001. Hydrologic-response simulations for the R-5 catchment with a comprehensive physics-based model. Water Resour. Res. 37, 999–1013.

Weiler, M., McDonnell, J., 2004. Virtual experiments: a new approach for improving process conceptualization in hillslope hydrology. J. Hydrol. 285, 3–18.

Winter, T.C., 1999. Relation of streams, lakes, and wetlands to groundwater flow systems. Hydrogeol. J. 7, 28–45.